NASA/CR—2015-218716

Far-Field Acoustic Power Level and Performance Analyses of F31/A31 Open Rotor Model at Simulated Scaled Takeoff, Nominal Takeoff, and Approach Conditions

Technical Report I

Dave Sree
Tuskegee University, Tuskegee, Alabama

May 2015

NASA STI Program . . . in Profile

Since its founding, NASA has been dedicated to the advancement of aeronautics and space science. The NASA Scientific and Technical Information (STI) Program plays a key part in helping NASA maintain this important role.

The NASA STI Program operates under the auspices of the Agency Chief Information Officer. It collects, organizes, provides for archiving, and disseminates NASA's STI. The NASA STI Program provides access to the NASA Technical Report Server—Registered (NTRS Reg) and NASA Technical Report Server—Public (NTRS) thus providing one of the largest collections of aeronautical and space science STI in the world. Results are published in both non-NASA channels and by NASA in the NASA STI Report Series, which includes the following report types:

- TECHNICAL PUBLICATION. Reports of completed research or a major significant phase of research that present the results of NASA programs and include extensive data or theoretical analysis. Includes compilations of significant scientific and technical data and information deemed to be of continuing reference value. NASA counter-part of peer-reviewed formal professional papers, but has less stringent limitations on manuscript length and extent of graphic presentations.

- TECHNICAL MEMORANDUM. Scientific and technical findings that are preliminary or of specialized interest, e.g., "quick-release" reports, working papers, and bibliographies that contain minimal annotation. Does not contain extensive analysis.

- CONTRACTOR REPORT. Scientific and technical findings by NASA-sponsored contractors and grantees.

- CONFERENCE PUBLICATION. Collected papers from scientific and technical conferences, symposia, seminars, or other meetings sponsored or co-sponsored by NASA.

- SPECIAL PUBLICATION. Scientific, technical, or historical information from NASA programs, projects, and missions, often concerned with subjects having substantial public interest.

- TECHNICAL TRANSLATION. English-language translations of foreign scientific and technical material pertinent to NASA's mission.

For more information about the NASA STI program, see the following:

- Access the NASA STI program home page at http://www.sti.nasa.gov

- E-mail your question to help@sti.nasa.gov

- Fax your question to the NASA STI Information Desk at 757-864-6500

- Telephone the NASA STI Information Desk at 757-864-9658

- Write to:
  NASA STI Program
  Mail Stop 148
  NASA Langley Research Center
  Hampton, VA 23681-2199

NASA/CR—2015-218716

Far-Field Acoustic Power Level and Performance Analyses of F31/A31 Open Rotor Model at Simulated Scaled Takeoff, Nominal Takeoff, and Approach Conditions

Technical Report I

Dave Sree
Tuskegee University, Tuskegee, Alabama

Prepared under Contract NNC13BA10B

National Aeronautics and
Space Administration

Glenn Research Center
Cleveland, Ohio 44135

May 2015

Acknowledgments

The present work was sponsored by the NASA Environmentally Responsible Aviation Project Propulsion subtask, with Ken Suder as Project Monitor. This work was performed under the Universities Space Research Association (USRA) Advanced Research and Technology Support Task Order, IDIQ Subcontract Number 04555-014 (Prime Contract Number NNC13BA10B) for NASA Glenn Research Center (NASA GRC). The support from USRA and Acoustics Branch at NASA GRC is greatly appreciated. The author would like to thank Dr. David B. Stephens of Acoustics Branch for all his help, suggestions, and fruitful discussions.

Level of Review: This material has been technically reviewed by NASA technical management.

Available from

NASA STI Program
Mail Stop 148
NASA Langley Research Center
Hampton, VA 23681-2199

National Technical Information Service
5285 Port Royal Road
Springfield, VA 22161
703-605-6000

This report is available in electronic form at http://www.sti.nasa.gov/ and http://ntrs.nasa.gov/

Preface

There are two parts to the technical aspects of the task under this Universities Space Research Association (USRA) subcontract number 04555-014. The first part involves performing and documenting the far-field acoustic (sound) power level and system performance analyses of open rotor model F31/A31 at simulated scaled takeoff, nominal takeoff, and approach flight conditions based on data obtained from low-speed wind tunnel (LSWT) tests at NASA Glenn Research Center (NASA GRC). The second part involves performing and documenting the near-field acoustic power level analysis of the same model at simulated cruise conditions based on data obtained from high-speed wind tunnel (SWT) tests at NASA GRC. The nonproprietary portions of the test data were provided by NASA GRC to perform the analyses. This subcontractor's report on the first part of the task is provided in the form of *Technical Report I* which consists of model's relevant sound power level and performance results from the analyses and their detailed discussions. The technical report is included as an attachment to this summary. The deliverables, namely, revised technical report, data analysis codes, spreadsheets of results, tables, figures, etc. will be shipped to the technical monitor at NASA GRC in electronic form at the end of the contract period.

Far-Field Acoustic Power Level and Performance Analyses of F31/A31 Open Rotor Model at Simulated Scaled Takeoff, Nominal Takeoff, and Approach Conditions

Technical Report I

Dave Sree
Tuskegee University
Tuskegee, Alabama 36088

Summary

Far-field acoustic power level and performance analyses of open rotor model F31/A31 have been performed to determine its noise characteristics at simulated scaled takeoff, nominal takeoff, and approach flight conditions. The nonproprietary parts of the data obtained from experiments in 9- by 15-Foot Low-Speed Wind Tunnel (9×15 LSWT) tests were provided by NASA Glenn Research Center to perform the analyses. The tone and broadband noise components have been separated from raw test data by using a new data analysis tool. Results in terms of sound pressure levels, acoustic power levels, and their variations with rotor speed, angle of attack, thrust, and input shaft power have been presented and discussed. The effect of an upstream pylon on the noise levels of the model has been addressed. Empirical equations relating model's acoustic power level, thrust, and input shaft power have been developed. The far-field acoustic efficiency of the model is also determined for various simulated flight conditions. It is intended that the results presented in this work will serve as a database for comparison and improvement of other open rotor blade designs and also for validating open rotor noise prediction codes.

Nomenclature

A_a	Reference rotor annular area
AOA	Angle of attack
APP	Approach
BSA	Blade-pitch setting angles
c_0	Speed of sound
C_{ac}	Acoustic power coefficient
C_{sp}	Input shaft power coefficient
C_T	Net thrust coefficient
d	Sideline distance
D	Reference rotor diameter
FFT	Fast Fourier Transform
J	Advance ratio
M_0	Freestream Mach number
N	Rotor speed (revolutions per unit time)
NTO	Nominal takeoff
OAPWL	Overall power watt level
OASPL	Overall sound pressure level
$\overline{p'^2}(d,\theta_g)$	Time-averaged mean-squared pressure
P_{ac}	Measured acoustic power
P_{ref}	Reference acoustic power
P_{sp}	Input shaft power
P_{spb}	Input shaft power per blade
PWL	Power watt level
R^2	Goodness-of-fit parameter
SPL	Sound pressure level
STO	Scaled takeoff
T	Net thrust
V_0	Freestream velocity
η_p	Propulsion efficiency
Π	Acoustic power level
ρ_0	Fluid density
θ_e	Acoustic emission angle
θ_g	Geometric angle

1.0 Introduction

The term "open rotor" refers to unducted counter-rotating dual rotors (propellers) which are being considered as propulsion devices for future aircraft (Refs. 1 and 2). Open rotors are also known as "propfans." Open-rotor propulsion technology is now being developed as a viable alternative to modern day turbofan engines mainly because of predicted fuel economy benefits and improved performance (Ref. 3). However, high noise levels associated with open rotors pose both environmental and technological challenges. These include community noise around airports, passenger discomfort, aircraft structural integrity, and meeting stringent federal noise regulations.

NASA Glenn Research Center (NASA GRC), in collaboration with the U.S. aircraft industry, has been conducting both analytical and experimental research studies to address this noise issue and to develop improved open rotor systems (Ref. 4). Tests on scale-model systems have been conducted in low- and high-speed wind tunnels at NASA GRC to understand the noise mechanisms and evaluate the acoustic performance of open rotors. Large amounts of both far-field and near-field acoustic data have been collected during an extensive test campaign in 2011 to determine the noise levels under various simulated flight conditions (Refs. 5 to 7). The far-field measurements were acquired on a 2.4-diameter (about 5 ft) sideline in the 9×15 LSWT and are the subject of the present report. This measurement distance is considered adequate for the sound to propagate as spherical waves. The near-field measurements were made on a sideline as close as 0.18 diameters (about 4.4 in.) in the 8- by 6-Foot (high speed) Supersonic Wind Tunnel (SWT) and are the subject of a companion report. The open rotor model used for testing was a one-fifth scale model having a so-called "historical" baseline blade set made of carbon fiber composite with a metal spar. This blade set is designated as "F31/A31" and serves as a nonproprietary baseline design for comparison with other blade designs (Refs. 5 to 7).

Far-field acoustic tests on the model were carried out in the 9×15 LSWT tunnel at NASA GRC to study its noise characteristics at simulated scaled takeoff (STO), nominal takeoff (NTO), and approach (APP) flight conditions. The expected takeoff speed for an aircraft equipped with open rotor was expected to be about Mach 0.25, while the 9×15 LSWT tunnel can only reliably reach about Mach 0.20 depending on ambient conditions. Thus "nominal takeoff" blade pitch settings correspond to producing 100 percent of takeoff thrust at 100 percent rotor speed with Mach 0.20 freestream. "Scaled takeoff" conditions are a lower tip speed blade pitch setting that would produce takeoff thrust at 100 percent rotor speed when extrapolated to a freestream speed of Mach 0.25. Then, at Mach 0.20, scaled takeoff will correspond to 64 percent of takeoff thrust at 80 percent shaft speed. Tests were conducted at various rotor speeds, angles of attack (AOA), and freestream Mach numbers (M_0) to conduct a parametric study on model noise levels. A pylon was also installed in some tests to determine its effect on the noise levels. The F31/A31 blades are being used to validate open rotor noise prediction codes as well as to improve acoustic and aerodynamic performance of current and future blade designs.

An initial investigation of the test data of F31/A31 model has been reported by Elliott (Ref. 5), and most recently by Stephens (Ref. 6), in terms of narrowband noise spectra, sound pressure levels (SPL) and power watt levels (PWL) at STO, NTO, and APP flight conditions. Some comparisons were also made to understand the noise effects of pylon installation and AOA changes. These investigations were based on the overall noise levels only. No attempts were made to separate the tone and broadband noise components from raw test data. They were estimated from the overall noise spectrum by chopping off the spectrum at the base of peaky "tones" and assuming the remaining part as the "broadband." No proper data processing tools were available at the time to separate tone and broadband noise.

It is known that the open rotor total (or overall) noise consists of both tonal and broadband components. (The terms "total" and "overall," and "tonal" and "tone," will be used interchangeably in this report.) The determination of tonal and broadband noise components from raw acoustic test data is very important for properly assessing the noise control parameters and also for validating the open rotor noise prediction codes (Refs. 8 to 11). A new data processing method developed by Sree (Ref. 12) is now available to separate the tonal and broadband noise (spectral) components from raw experimental data of open rotors. This method will be applied to examine the tone and broadband noise levels of F31/A31 model.

The main purpose of the present work is to analyze the far-field experimental data available on F31/A31 and report separately the tone and broadband noise results together with total noise. The test data, portions of which are deemed nonproprietary, were provided by NASA GRC to perform the task. The noise levels will be expressed in terms of SPLs and PWLs at simulated STO, NTO, and APP conditions. Variations of the noise levels with rotor speed, AOA changes, and input shaft power will be studied. The results will also include the effects of pylon installation on model's noise. The noise levels will be examined to obtain correlations with model performance variables, such as rotor speed, thrust, and input shaft power. Model performance evaluation will also be made in terms of nondimensional parameters and empirical equations will be developed. It is hoped that the results presented here will serve as a valuable database for comparing other open rotor blade designs with F31/A31 and also for validating open rotor noise simulation codes.

2.0 F31/A31 Model and the Test Rig

A detailed description of F31/A31 model and the test rig is given by Elliot (Ref. 5) and Stephens (Ref. 6). However, a few salient features of the model will be worth repeating here. The F31/A31 model has two counter-rotating rotors. The axial distance between their pitch axes is 19.9 cm (7.8 in.). The forward rotor is approximately 65.2 cm (25.7 in.) in diameter and has 12 blades whereas the aft rotor is approximately 63.0 cm (24.8 in.) in diameter and has 10 blades. The hub diameter of the forward rotor is approximately 26.6 cm (10.5 in.) and that of the aft rotor is 24.6 cm (9.7 in.). The pitch of the rotor blades could be adjusted to provide different simulated flight conditions. The blade-pitch setting angles (BSA) of forward and aft rotors for the three flight conditions considered are as shown in Table 1. These BSAs were chosen in order to obtain the best aerodynamic performance of the system at a given shaft speed and flight condition (Ref. 5). It should be noted here that a change in blade-pitch angles means a change in flight condition.

For all the tests conducted in the 9×15 LSWT, the F31/A31 model was mounted on a test rig called the "Open Rotor Propulsion Rig (ORPR)" in a simulated pusher-type arrangement (Refs. 5 and 6). The turbines within the test rig were fed by high pressure air at about 20 atm (300 psi) to turn the rotor blades. The drive rig was mounted on a turntable to provide angle of attack (AOA) changes relative to longitudinal axis of the model. The test rig had the capability to install a pylon upstream of the forward rotor to study its effect on overall noise development. Photographs of the model and the test rig installed in the LSWT, with and without pylon, are shown in Figures 1(a) and (b), respectively.

TABLE 1.—BLADE-PITCH SETTING ANGLES (BSA) FOR THE THREE SIMULATED FLIGHT CONDITIONS

Simulated flight condition	BSA (Forward/Aft)
Scaled takeoff (STO)	43.0°/43.5°
Nominal takeoff (NTO)	40.1°/40.8°
Approach (APP)	33.7°/35.7°

(a) With pylon

(b) Without pylon

Figure 1.—Photographs of F31/A31 model and ORPR test rig installed in 9×15 LSWT; (a) with pylon; (b) without pylon; (Courtesy: Acoustics Branch, NASA GRC).

3.0 Test Configurations

The test configurations for the model are summarized as given in Table 2 where test runs were made at various rotor speeds and angles of attack, with and without pylon installation, using a freestream $M_0 = 0.20$. The tests that were performed (indicated by "y" in Table 2) had both rotors running at approximately the same speed. The rotor speeds were taken as the percentage of corrected design speed which was 6530 rpm. A few limited tests were conducted with $M_0 = 0.22$ but they are not considered in the present work.

TABLE 2.—TEST CONFIGURATIONS FOR F31/A31 OPEN ROTOR MODEL IN LSWT
[Cells showing "y" represent tests that were performed in the current study.]

Simulated Flight Condition	% Rotor Design Speed	With Pylon			Without Pylon		
		AOA = 0°	AOA = 3°	AOA = 8°	AOA = 0°	AOA = 3°	AOA = 8°
	68.7				y		
	71.4				y		
	80.0				y		
Scaled Takeoff	84.0				y		
(STO)	89.3				y		
M_0 = 0.2	92.7				y		
	93.9				y		
	94.3				y		
	97.8				y		
	70.7	y	y	y	y	y	y
Nominal Takeoff	80.5				y		
(NTO)	85.0	y	y	y	y	y	y
M_0 = 0.2	93.0	y			y		
	96.5	y	y		y	y	y
	98.5	y			y		
	85.5	y	y	y	y	y	y
Approach	96.7	y	y	y	y	y	y
(APP)	103.5	y	y	y	y	y	y
M_0 = 0.2	110.5	y			y		
	114.4	y			y		

4.0 Far-Field Sideline Acoustic Measurements

The far-field sideline acoustic measurements were made using a traversing microphone probe on a track parallel to and 1.524 m (5 ft) away from the model (centerline) longitudinal axis (Refs. 5 and 6). The track can be seen in Figure 1(b). Data were taken at 18 positions, or stops, as the traverse moved from rear side to front side of the model during each test. At each stop, 3 million samples were acquired at a sampling rate of 200 kHz. The 18 traversing microphone stops are depicted in Figure 2 and the corresponding calculated geometric angles, θ_g, and acoustic emission angles (Ref. 6), θ_e, relative to the aft rotor pitch-change axis at $M_0 = 0.20$ and a sideline distance, d = 1.524 m are listed in Table 3. The angles are measured with respect to the longitudinal axis of the model from the front.

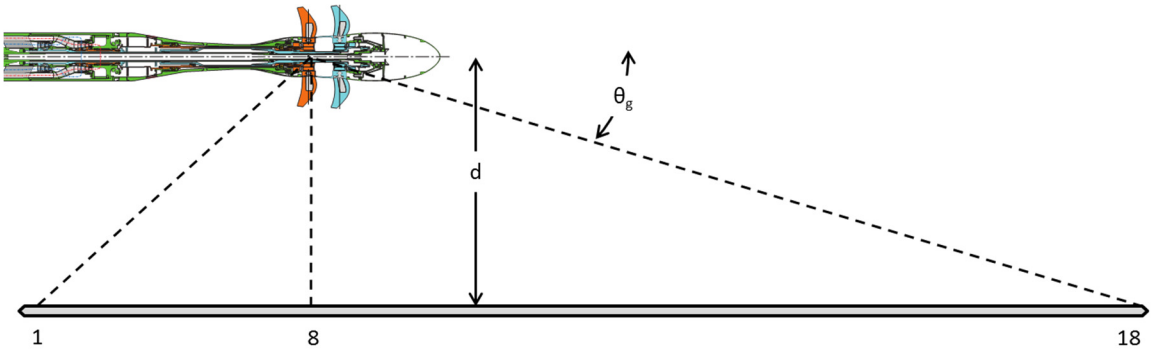

Figure 2.—Sketch depicting microphone stops relative to aft rotor of F31/A31 model in 9×15 LSWT; (Courtesy: Acoustics Branch, NASA GRC).

TABLE 3.—MICROPHONE STOPS AND CORRESPONDING STREAMWISE LOCATIONS, GEOMETRIC AND ACOUSTIC EMISSION ANGLES RELATIVE TO AFT ROTOR PITCH CHANGE AXIS AT $M_0 = 0.20$

Traversing Microphone Stop Number	Streamwise Location (meters)	Geometric Angle, θ_g (degree)	Acoustic Emission Angle, θ_e (degree)
1	-1.81	140.0	132.6
2	-1.52	135.0	126.9
3	-1.17	127.5	118.3
4	-0.88	119.9	110.0
5	-0.63	112.6	101.9
6	-0.41	105.0	93.9
7	-0.20	97.5	86.1
8	0.00	90.0	78.5
9	0.20	82.5	71.0
10	0.41	75.0	63.9
11	0.63	67.4	56.8
12	0.88	60.1	50.1
13	1.17	52.5	43.4
14	1.52	45.0	36.9
15	1.99	37.5	30.5
16	2.64	30.0	24.3
17	3.68	22.5	18.1
18	4.79	17.6	14.2

5.0 Results and Discussions

The results and discussions of computed far-field noise levels from the test data for the F31/A31 model at different simulated flight conditions are presented in this section. As mentioned earlier, the new data processing technique was used to separate the tone and broadband noise components from raw test data. Noise levels of each component were computed in terms of SPLs and PWLs and as a function of rotor speed, thrust, and AOA changes. The results of the variations of noise levels at different simulated flight conditions and the effects of pylon installation are presented and discussed. Model performance characteristics are also studied. The necessary data required for performance evaluation were obtained from run logs of the model test in LSWT. Correlations of thrust and overall PWL (OAPWL) with input shaft power are also presented.

5.1 Narrowband Noise Spectra

As stated earlier, the total, tonal, and broadband narrowband noise spectra were first determined using the method developed by Sree (Ref. 12). The spectral analysis of the data was performed using a time history length of 15 sec (3 million samples) with a Fast Fourier Transform (FFT) block size of 16,384 points, giving a frequency resolution of 12.2 Hz at 200 kHz sampling rate. In order to avoid the interference of wind tunnel background noise, particularly at low rotor speeds, the raw data was pre-processed using a 500 Hz to 50 kHz band-pass filter before the spectral analysis was carried out. The 9×15 LSWT noise interference has already been reported earlier by Elliott (Ref. 5), Stephens (Ref. 6), and Woodward, et al. (Ref. 8).

An example of the narrowband spectra of the total (blue) noise and its corresponding tonal (red) and broadband (green) components is shown in Figure 3. These spectra were computed from the far-field acoustic data measured at microphone stop no. 8 which is at 90° geometric (or 78.5° acoustic) directivity angle with respect to aft rotor pitch axis. The test case was 85 percent rotor design speed at simulated NTO condition without pylon and AOA = 0°. The spectral values are given in SPL (dB) as a function of frequency, in Hz.

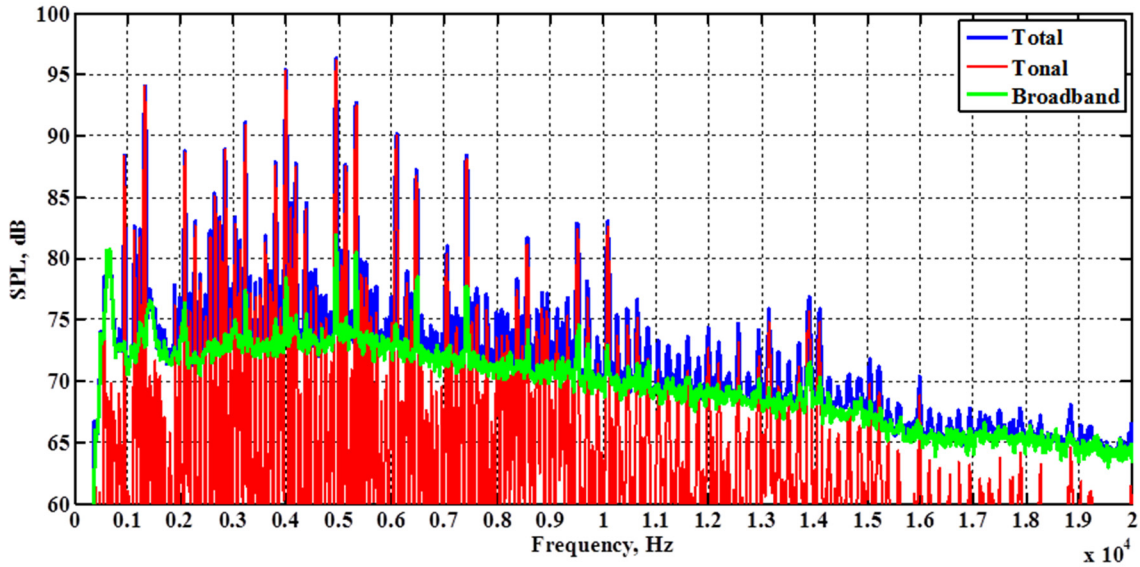

Figure 3.—Narrowband noise spectra of total, tonal, and broadband components (stop no. 8) at simulated NTO condition without pylon; 85 percent rotor design speed, AOA = 0°.

It is seen from this example that the tone noise is dominant in the 1 to 10 kHz range. The tone and broadband noise components are reasonably well separated except for a few spikes in the broadband spectrum (green curve in Fig. 3). Notice that these spike levels are well below their corresponding (major) tonal levels. The spikes are attributed to random phase shifts and modulations in narrow tonal frequencies in the measured signal due to unsteadiness or jitter in rotor speeds, particularly at higher shaft speeds. Measured signals also get distorted by other extraneous effects. The new data processing technique by Sree (Ref. 12) is not able to eliminate the spikes completely. This is one of the limitations of the new technique, particularly at higher shaft speeds with jitter, as reported by Sree and Stephens (Ref. 13).

5.2 Thrust Versus Speed Relation—Effect of AOA and Pylon

Before considering the results of SPLs and PWLs, it is necessary to present the thrust versus speed relation for the model first. The net (or total) thrust was measured by running both forward and aft rotors at the same speed. The net thrust as a function of percent rotor design speed is shown in Figures 4 for AOA = 0°, 3°, and 8° at simulated STO, NTO, and APP conditions. Figure 4(a) shows the results when pylon was present and Figure 4(b) the results without it. It should be noted that all STO runs were made without pylon at AOA = 0° only (see Table 2). The results show that, at a given rotor speed and flight condition, there are very minor changes in the thrust value when AOA is changed.

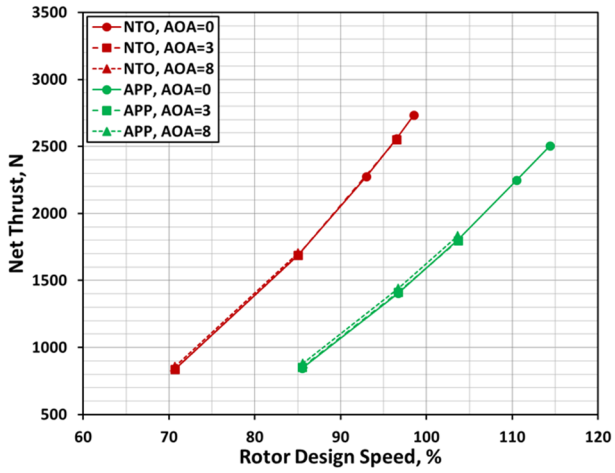

(a) With pylon

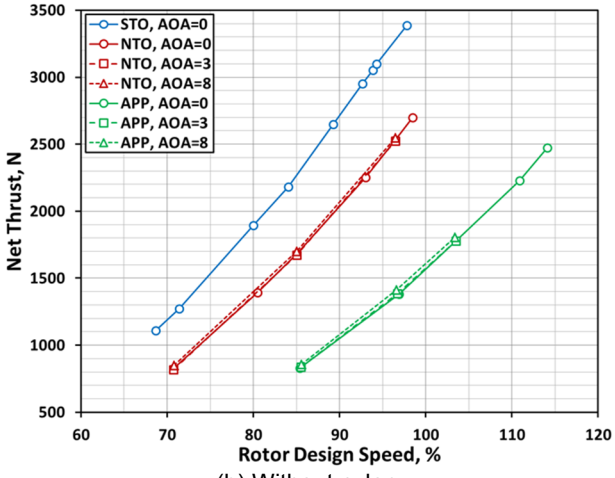

(b) Without pylon

Figure 4.—Net thrust as a function of rotor speed at AOA = 0°, 3°, and 8° for simulated STO, NTO, and APP conditions; (a) with pylon and (b) without pylon.

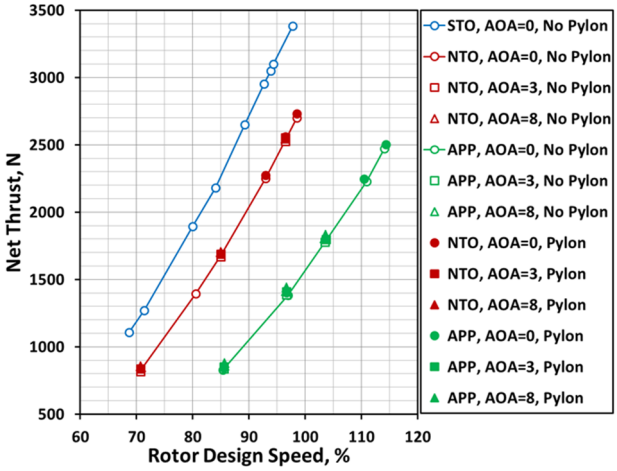

Figure 5.—Comparison of net thrust versus rotor design speed for AOA = 0°, 3°, and 8° at STO, NTO, and APP conditions with and without pylon.

The results shown in Figure 4 when combined together and replotted as shown in Figure 5, also reveal that the presence of pylon and/or the AOA change brings only minor differences in the thrust value for a given rotor speed and flight condition (or blade-pitch setting). It is also noticed that each blade-pitch setting has a different thrust value for a given rotor speed, or conversely, each flight (or BSA) case has a different rotor speed at a given thrust value.

5.3 Integrated Sound Pressure Levels

The integrated sound pressure levels of the total, tone, and broadband noise at simulated flight conditions are also computed and compared. The integration was carried out using their respective narrowband spectral values from 500 Hz to 50 kHz. The main purpose of comparison of integrated SPL results here is to determine the effects of AOA change and pylon presence. Only the NTO case is considered here. The STO case had no data with pylon or AOA change and hence is not included. Results for the simulated APP condition were found to be similar.

5.3.1 Effect of AOA

Figure 6 shows a comparison of the integrated SPLs of the overall and the corresponding tonal and broadband signals for the case of 85 percent rotor design speed at simulated NTO condition without pylon. Figure 6(a) shows the integrated SPLs of the overall signal (also referred to as the overall SPL or OASPL) as a function of acoustic emission angle relative to aft rotor pitch axis (see Table 3) for AOA = 0°, 3°, and 8°. The results show that the noise level increases as the AOA increases. Further investigation showed that, at higher speeds, the noise difference between 0° and 3° becomes smaller compared to that between 3° and 8°. The results of the integrated SPLs of the corresponding tone and broadband noise components also had similar characteristics, as shown in Figures 6(b) and (c), respectively.

5.3.2 Effect of Pylon

A comparison of the noise levels to study the effect of pylon installation is made in Figure 7. It shows the variation of integrated SPLs of the total and the corresponding tone and broadband noise components as a function of acoustic emission angle for the case with and without pylon. These results are again from data taken at 85 percent rotor design speed for the simulated NTO condition with AOA = 0°. The results show that the presence of pylon causes a 1 to 3 dB increase in each noise component. A separate study showed that the difference in broadband noise levels with and without pylon was becoming smaller at higher speeds. Similar results were found at other AOAs and rotor speeds also.

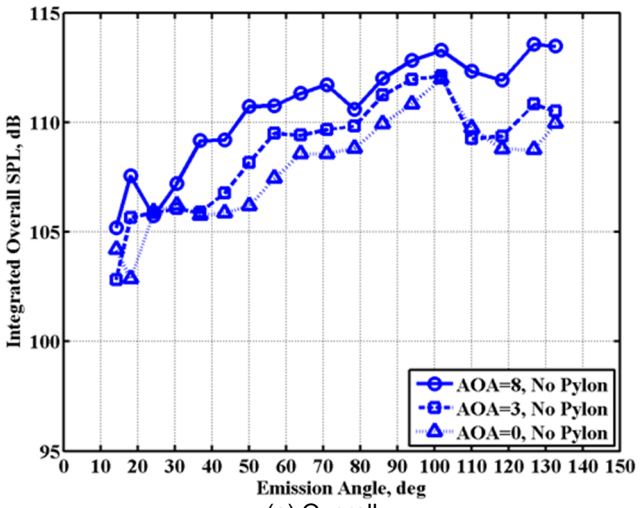

(a) Overall

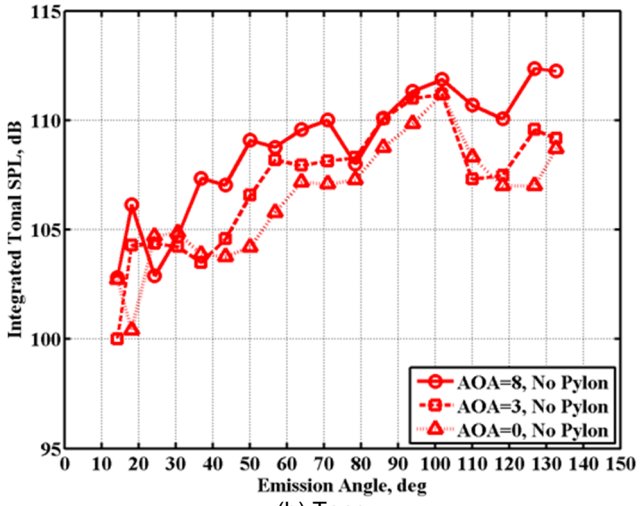

(b) Tone

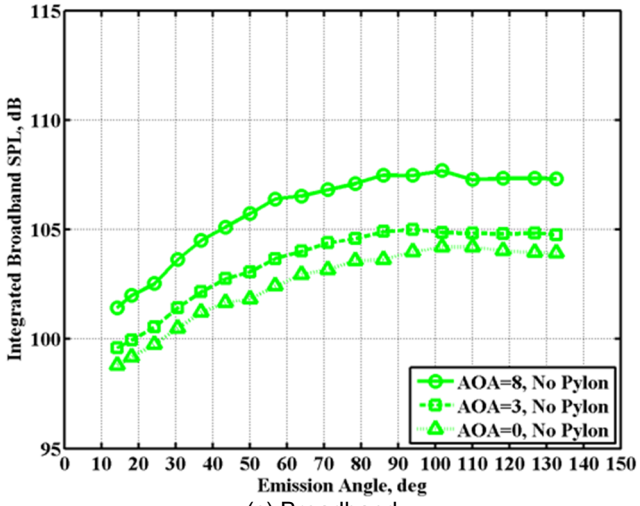

(c) Broadband

Figure 6.—Comparison of integrated SPLs of (a) overall and the corresponding (b) tone, and (c) broadband noise components as a function of acoustic emission angle at simulated NTO condition without pylon; 85 percent rotor design speed.

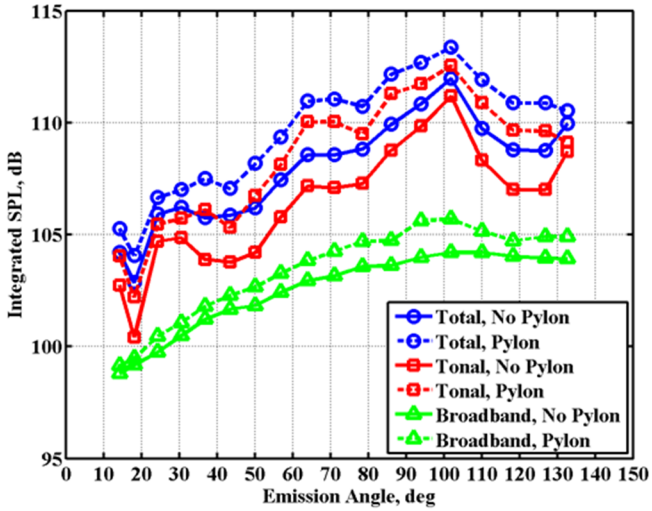

Figure 7.—Comparison of integrated SPLs of total and the corresponding tonal and broadband noise components as a function of acoustic emission angle at simulated NTO condition with and without pylon; 85 percent rotor design speed, AOA = 0°.

5.3.3 Effect of Flight Condition

The integrated SPLs of the noise levels for a given rotor speed and thrust are also compared to understand the relative differences among the three simulated flight conditions. Since the data obtained for the simulated STO condition were only for AOA = 0° without pylon, the comparison made here will be with similar data at NTO and APP conditions also.

5.3.3.1 Comparison at a Given Rotor Speed

Figure 8 shows a comparison of the integrated SPLs of the overall and the corresponding tonal and broadband signals for the three simulated flight conditions at a given rotor design speed of 85 percent, without pylon and AOA = 0°, in each case. Figure 8(a) shows the integrated SPLs of the overall noise as a function of acoustic emission angle. The results show that the SPLs of the total noise at STO are higher than the SPLs at NTO which, in turn, are higher than those at APP. This is the same order in which the thrust increases for a given rotor speed (Fig. 5). Similar results are obtained for the tone and broadband noise components also as shown in Figures 8(b) and (c), respectively.

5.3.3.2 Comparison at a Given Thrust

Figure 9 shows a comparison of the integrated SPLs of the overall and the corresponding tonal and broadband signals for the three simulated flight conditions at a given net thrust of 2224 N (500 lb), without pylon and AOA = 0°, in each case. Figure 9(a) shows the integrated SPLs of the overall noise as a function of acoustic emission angle. The results show that the overall noise levels for the three cases are generally between 105 and 116 dB with larger values occurring around higher emission angles. The tonal results, given in Figure 9(b), shows generally higher SPLs for APP than for NTO and STO. The STO values are lower than NTO values for the large part. However, a separate study showed that at lower thrust values the tonal SPLs were fluctuating (1 to 5 dB) with APP being generally higher. The broadband noise results are shown in Figure 9(c) where the STO levels are higher than those for NTO or APP, but NTO values are higher than APP values. At lower thrust values, the broadband SPL differences between NTO and APP cases were found to be less than 2 dB.

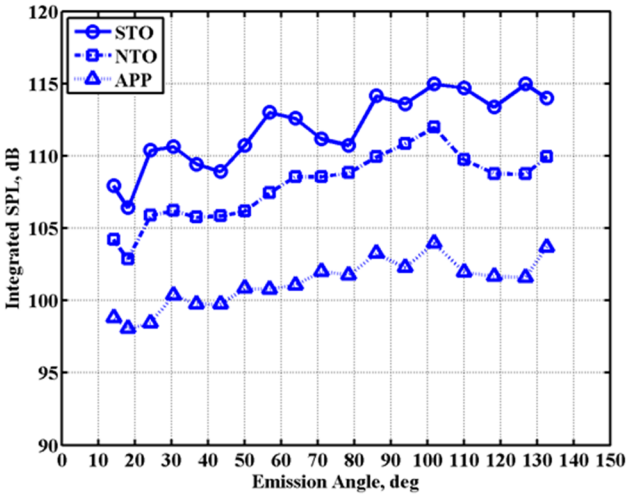

(a) Overall

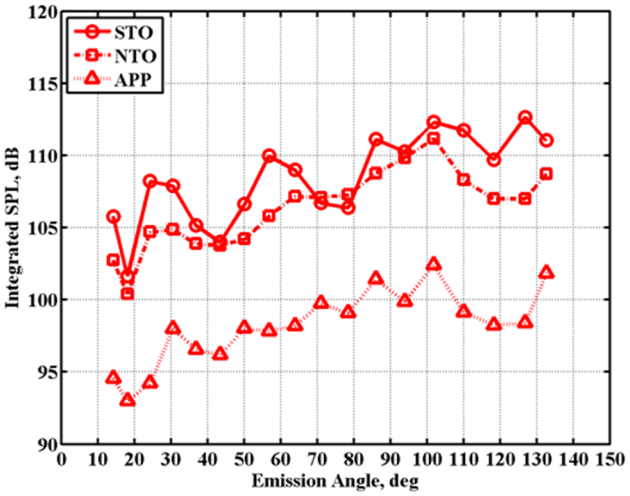

(b) Tone

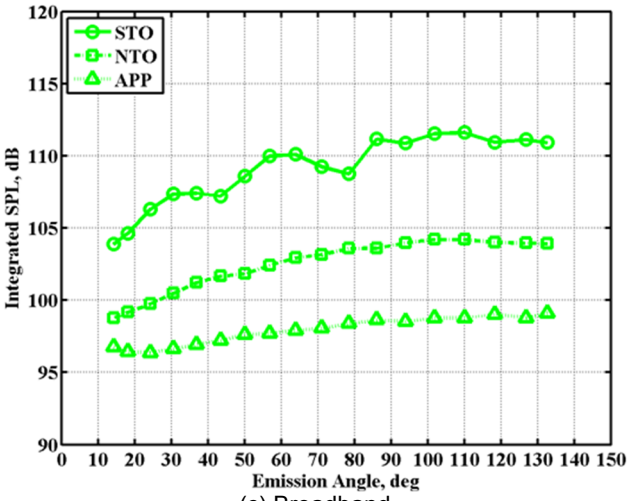

(c) Broadband

Figure 8.—Comparison of integrated SPLs of (a) overall and the corresponding (b) tone, and (c) broadband noise components as a function of acoustic emission angle at simulated STO, NTO, and APP conditions without pylon; 85 percent rotor design speed, AOA = 0°.

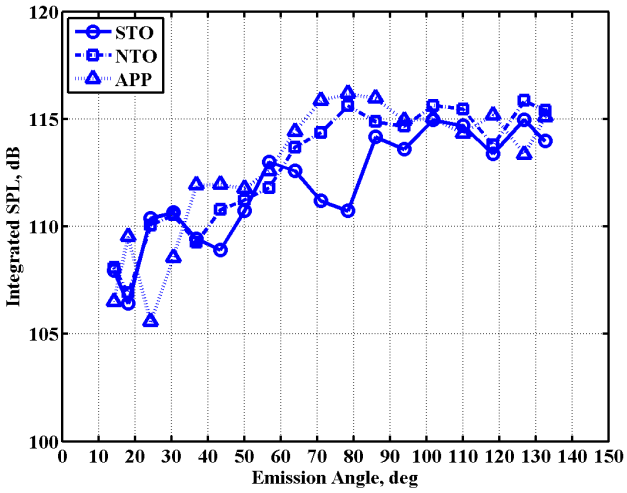

(a) Overall

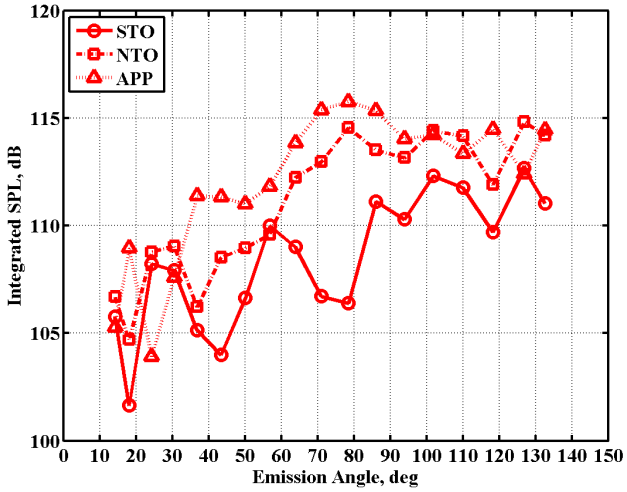

(b) Tone

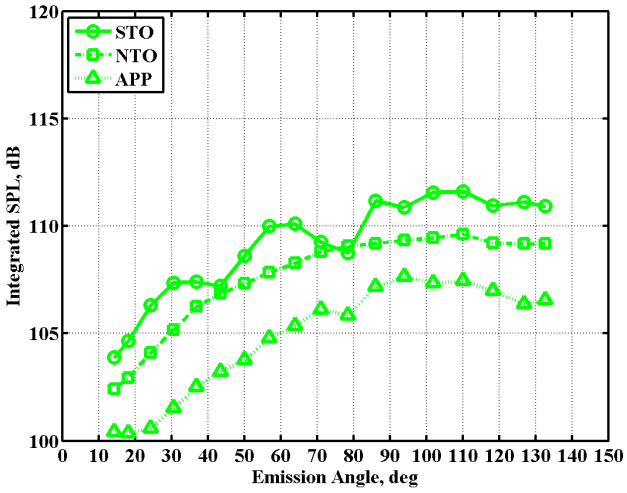

(c) Broadband

Figure 9.—Comparison of integrated SPLs of (a) overall and the corresponding (b) tone, and (c) broadband noise components as a function of acoustic emission angle at simulated STO, NTO, and APP conditions without pylon; 2224 N (500 lb) thrust, AOA = 0°.

5.4 Acoustic Power Levels

Sound or acoustic power is sonic energy per unit time and is measured in Watts (W). The sound power level, sometimes, is expressed as Power Watt Level (PWL) in dB unit. PWL is a logarithmic measure of the sound power level in comparison to a reference level of 10^{-12} W, i.e., $PWL_{dB} = 10 \log_{10} (P_{ac}/P_{ref})$ where P_{ac} = measured acoustic power in W and $P_{ref} = 10^{-12}$ W.

In this work, the acoustic power level, Π (or PWL), was calculated using the following equation which takes into account the tunnel or freestream Mach number effect (Ref. 14):

$$\Pi = \frac{2\pi d^2}{\rho_0 c_0} \int_0^{\pi} (1 - M_0 \cos\theta_e)^2 \frac{\overline{p'^2}(d, \theta_g)}{\sin\theta_e} d\theta_e$$

where

d	sideline distance from model centerline
ρ_0	ambient air density
c_0	speed of sound
M_0	tunnel or freestream Mach number
θ_e	acoustic or sound emission angle
θ_g	geometric (measurement) angle
$\overline{p'^2}(d,\theta_g)$	time-averaged sideline mean-squared pressure at measurement angle, θ_g

[Note: $\theta_e = \theta_g - \sin^{-1}(M_0 \sin\theta_g)$]

by assuming the measured sideline pressures were in the acoustic far-field. Spherical spreading was used to map the sideline measurement on to a constant radius arc. The acoustic intensity (Ref. 14) at each speed was calculated using the information from corresponding narrowband spectra and was integrated over frequencies between 500 Hz and 50 kHz. The intensity was assumed to be symmetric about the axis of the model and integrated over the portion of the spherical surface spanned by the sideline measurement angles. The upstream and downstream portion beyond the measurement angle was excluded from the calculation.

5.4.1 Overall PWL Versus Rotor Speed; Effect of AOA

Overall PWLs of the total noise were computed as a function of rotor speed for the three angles of attack considered both with and without pylon. Results are given in Figure 10. Figure 10(a) shows the results computed at AOA = 0°, 3°, and 8° for the STO, NTO, and APP conditions with pylon. (Note that the STO case had no data with pylon.) Similar results are shown in Figure 10(b) for the case without pylon. The results show that, in each flight case, there is very little difference in the overall PWL (less than 1 dB) for AOA = 0° and 3°, but that difference becomes 1 to 3 dB when AOA is increased to 8°. In general, for a given rotor speed, the overall PWL values for STO are higher than the values for NTO which, in turn, are higher than those for APP. Tone and broadband noise were found to have similar characteristics.

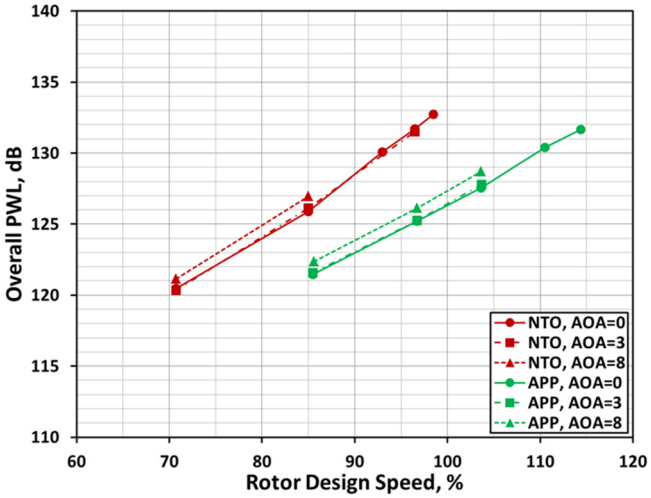

(a) With pylon

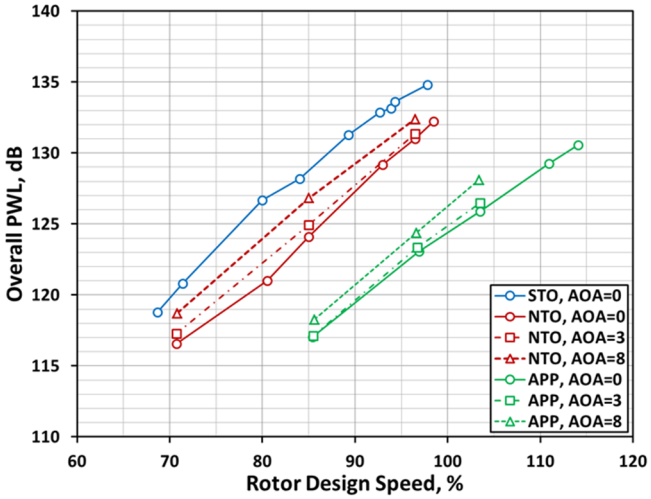

(b) Without pylon

Figure 10.—Overall PWL as a function of rotor speed at AOA = 0°, 3°, and 8° for simulated STO, NTO, and APP conditions; (a) with pylon and (b) without pylon.

5.4.2 PWLs of Noise Components; Effect of Pylon

The results in Figure 10, after careful examination, also show that there are differences in the overall PWL value when the pylon is present. These differences are shown in Figure 11(a) by replotting the results exclusively for the AOA = 0° case. These overall PWL results show that, in general, the PWL is higher when pylon is present. (STO case had no data with pylon.) The PWL difference starts at about 4 dB at lower rotor speeds and gradually decreases to about 1 dB or less at higher speeds for each simulated flight condition. A similar analysis was performed for the tonal and broadband noise components also and the results are shown in Figures 11(b) and (c), respectively. In the tonal case, the PWL difference when pylon is present starts at about 5 dB and gradually decreases to about 1 dB or less at higher speeds for a given simulated flight condition. In the broadband case, these differences are less than about 2 dB.

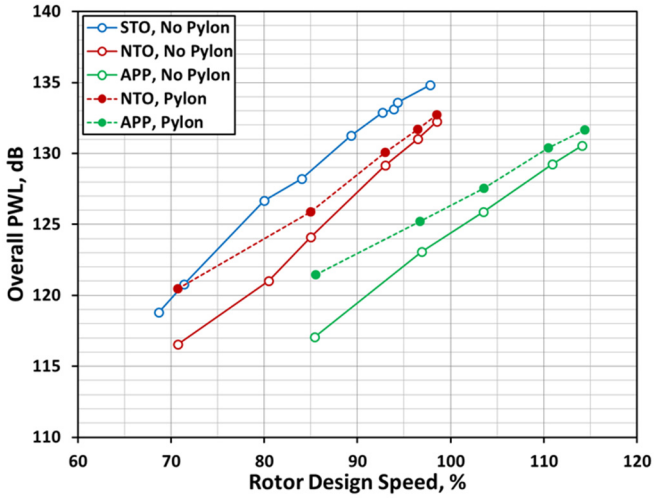

(a) Overall

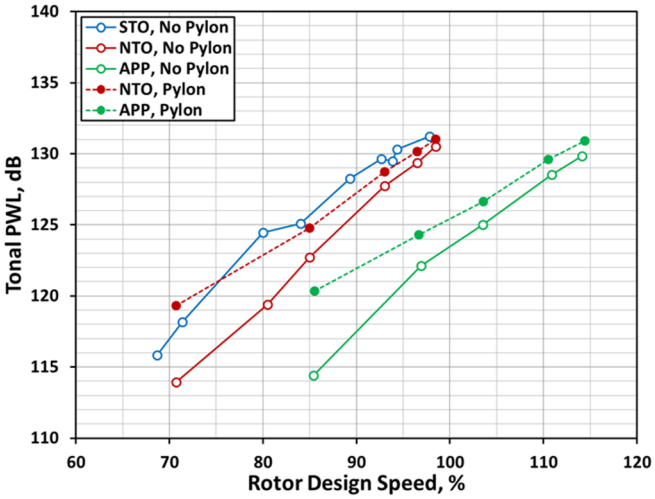

(b) Tonal

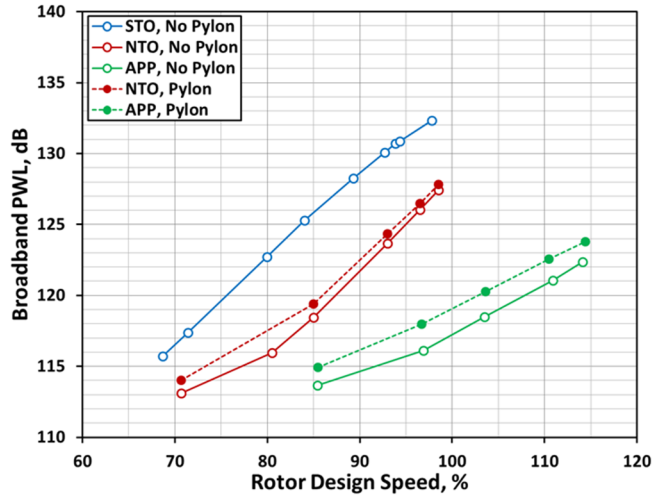

(c) Broadband

Figure 11.—Comparison of (a) overall and the corresponding (b) tonal and (c) broadband PWLs as a function of rotor design speed at simulated STO, NTO, and APP conditions with and without pylon; AOA = 0°.

5.4.3 Comparison of PWLs of Noise Components at a Given Flight Condition

The overall and the corresponding tonal and broadband PWLs together are once again presented separately for each simulated flight condition as shown in Figures 12. This helps to understand and visualize the relative contribution from tone and broadband noise to make up the total noise.

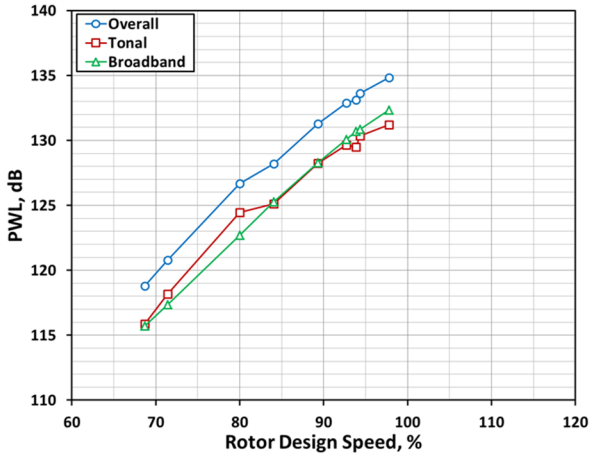

(a) STO

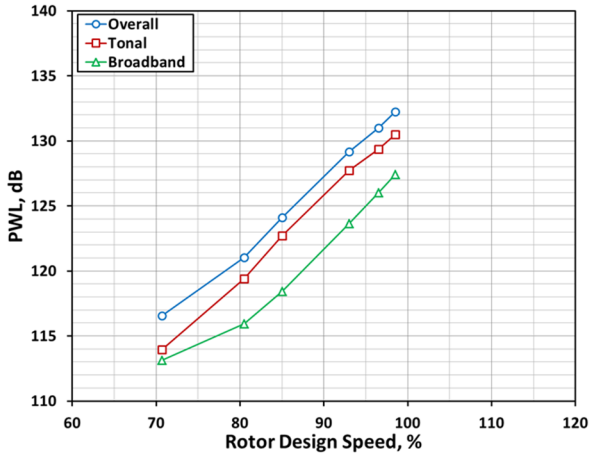

(b) NTO

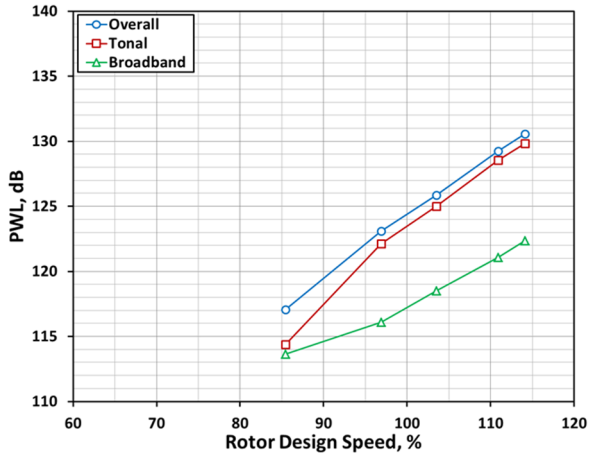

(c) APP

Figure 12.—Overall and the corresponding tonal and broadband PWLs as a function of rotor design speed at (a) STO, (b) NTO, and (c) APP; AOA = 0°, without pylon.

The results are given as a function of rotor design speed for AOA = 0°, without pylon, only. It is interesting to see that, in the STO case (Fig. 12(a)), the broadband levels become higher than the tonal levels for rotor speeds beyond about 82 percent. This could be due to thicker and more turbulent blade wakes or possibly flow separation occurring at higher blade-pitch setting at STO. This is not so in the NTO (Fig. 12(b)) or APP (Fig. 12(c)) case where the tonal levels are always higher than the broadband levels for any given rotor speed. Also it is seen that, in general, the noise levels (of each component) in STO case are higher than the levels in NTO which, in turn, are higher than those in APP case for a given rotor speed.

5.5 Acoustic Performance of F31/A31

The acoustic performance of open rotors is also of great concern in the open rotor research and design community. It is usually evaluated based on correlation between emitted acoustic power and a system performance variable, such as thrust or input shaft power. Here an attempt will be made to develop a correlation between overall PWL and input shaft power for F31/A31 model. Before considering this correlation, it is also important to study the variations of input shaft power with rotor speed, as well as thrust, for the model at all the simulated flight conditions. The study is given below.

5.5.1 Input Shaft Power Versus Rotor Speed

The variations input shaft power with rotor speed for the F31/A31 model at all the test conditions are shown in Figure 13. It is seen that the shaft power, for a given rotor speed and flight condition, is almost independent of AOA change and pylon presence. These results have similar characteristics to that of thrust versus rotor speed (Fig. 5). Also noticed is that each simulated flight condition has a different input shaft power value for a given rotor speed.

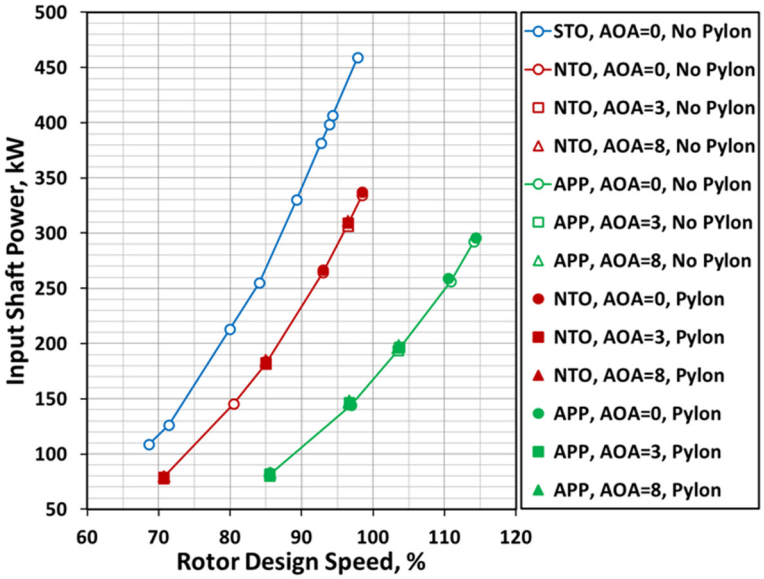

Figure 13.—Comparison of input shaft power versus rotor design speed at simulated STO, NTO, and APP conditions with and without pylon for AOA = 0°, 3°, and 8°.

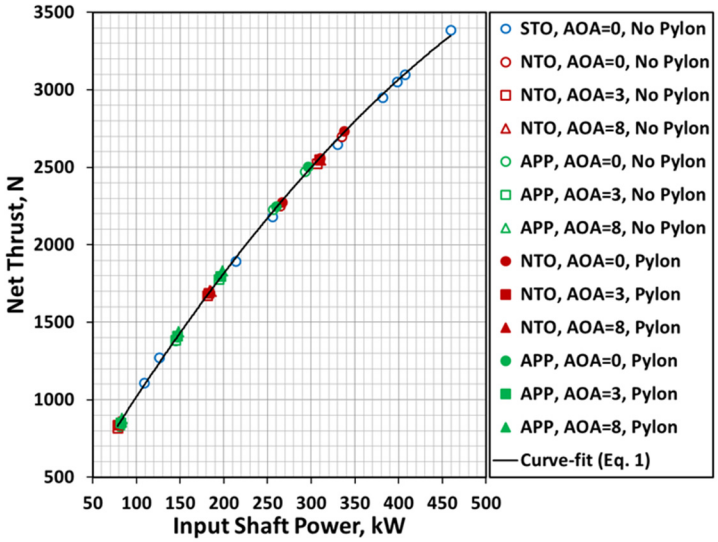

Figure 14.—Variation of net thrust with input shaft power at STO, NTO, and APP conditions with and without pylon for AOA = 0°, 3°, and 8°.

5.5.2 Thrust Versus Input Shaft Power

It is also important to know how thrust varies with shaft power for the model. The variations of net thrust with input shaft power from all the test cases are shown in Figure 14. The results exhibit a very good correlation between thrust and input shaft power for the F31/A31 model. From regression analysis, a polynomial curve-fit of the form:

$$T = - 0.0058\ P_{sp}^{2} + 9.7138\ P_{sp} + 104.7926 \quad (1)$$

with a goodness-of-fit parameter $R^2 = 0.9995$, has been determined. In the equation above, T stands for net or total thrust, in N, and P_{sp} for total input shaft power, in kW.

5.5.3 Overall PWL Versus Input Shaft Power

As mentioned before, STO, NTO, and APP comparison means comparison of different BSAs for the open rotor model. Several parameters can be used to establish correlation between acoustic power levels and model performance variables. Janardan and Gliebe (Ref. 15) found a good correlation between overall PWL (OAPWL) and input shaft power for one of the earlier open rotor models they tested. They suggested to use a plot of overall PWL as a function of shaft power per blade, or $\log_{10}$ (shaft power per blade), to obtain a good indication of blade loading for a given input shaft power. Both types of plots are presented in Figure 15 for the F31/A31 model. The results shown in the plots are for the case where AOA = 0°, without pylon, at simulated STO, NTO, and APP conditions. As seen from these results, a good correlation between OAPWL and input shaft power is observed. Using regression analysis, a power curve-fit of the form:

$$OAPWL = 104.2\ P_{spb}^{0.09} \quad (2)$$

with $R^2 = 0.99$ is found for the results in Figure 15(a), whereas a linear curve-fit of the form:

$$OAPWL = 24.8 \log_{10} (P_{spb}) + 102.2 \quad (3)$$

with $R^2 = 0.99$ is found for the results in Figure 15(b). In both of these equations, P_{spb} stands for input shaft power per blade, in kW, and OAPWL is in dB. Based on the actual results obtained in this work, the maximum error associated with these empirical equations is found to be less than 1.5 dB. Similar correlations can be obtained for tonal and broadband PWLs also.

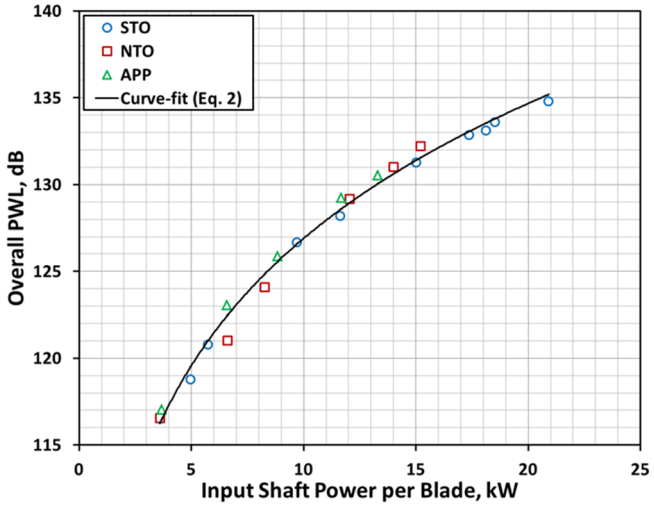

(a) OAPWL versus Shaft Power per Blade

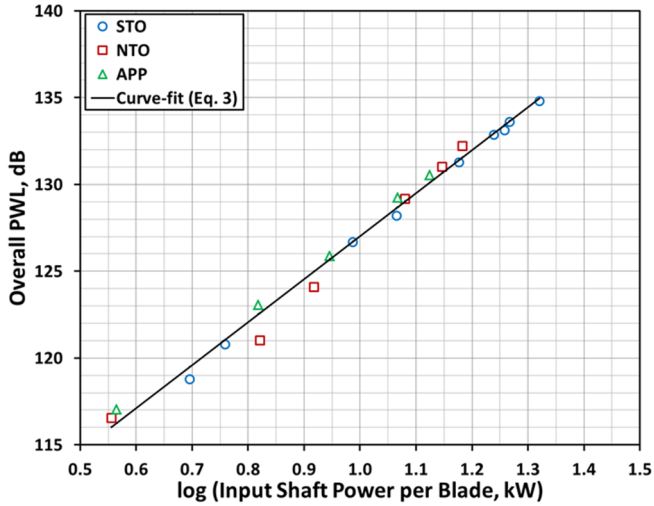

(b) OAPWL versus $\log_{10}$ (Shaft Power per Blade)

Figure 15.—Variation of OAPWL with input shaft power at STO, NTO, and APP conditions for AOA = 0° without pylon.

5.6 Acoustic Efficiency

The acoustic efficiency is defined as the ratio of the radiated acoustic power to the input shaft power where the radiated acoustic power is taken as the OAPWL (Refs. 15 and 16). Both powers are taken in kilowatt units in this work. Janardan and Gliebe (Ref. 15) came up with an acoustic efficiency of less than 0.1 percent for the F7A7 (8/8) open rotor blade design they tested. Hanson (Ref. 16) quotes typical acoustic efficiency values in the range of 0.02 to 0.05 percent for modern turbofan engines. [Huff (Ref. 17) reports that there has been considerable reduction (about 20 dB) in average noise levels for commercial aircraft since the 1960s.] Hanson also states that the significantly higher values for open rotors are attributed to the open tips and smaller number of blades.

Based on computed values in the present study, the acoustic efficiency for the F31/A31 model is found to be less than 0.007 percent for the BSAs at STO, NTO, and APP conditions, as shown in Figure 16. This order of magnitude reduction is presumably attributed to significant improvements in open rotor design compared to those since the mid 1980s. The results shown in this plot are for the case of AOA = 0°, without pylon, only.

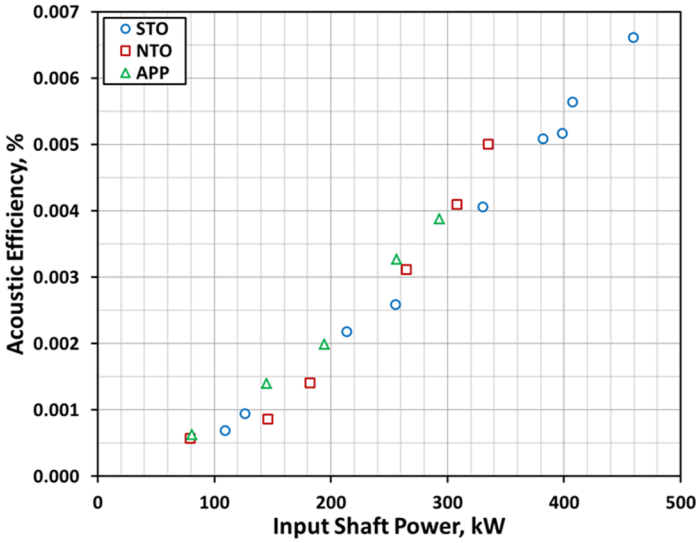

Figure 16.—Acoustic efficiency of F31/A31 model based on results from simulated STO, NTO, and APP conditions at AOA = 0° without pylon.

5.7 Nondimensional Plots of Model Performance

The F31/A31 open rotor model performance characteristics can also be visualized through some traditionally-used nondimensional parameters. Generalized empirical equations of model performance can be obtained by plotting these parameters in certain ways. The parameters used in this work are defined as follows:

Advance ratio (J): $J = V_0 / N D$

Thrust coefficient (C_T): $C_T = T / \rho_0 N^2 D^2 A_a$

Propulsion efficiency (η_p): $\eta_p = T V_0 / P_{sp}$

Input shaft power coefficient (C_{sp}): $C_{sp} = P_{sp} / \rho_0 N^3 D^3 A_a$

Acoustic power coefficient (C_{ac}): $C_{ac} = P_{ac} / \rho_0 N^3 D^3 A_a$

where

V_0	Freestream velocity	T	Net thrust
ρ_0	Fluid density	P_{sp}	Net input shaft power
N	Rotor speed (revs per unit time)	P_{ac}	Measured acoustic power
D	Reference rotor diameter	A_a	Reference rotor annular area

Note that the forward rotor was referenced for all the above calculations in this work.

Advance ratio (J) of a propeller (or rotor) is the ratio between the distance the propeller moves forward through the fluid medium during one revolution and the diameter of the propeller (Ref. 18). High advance ratio means high speed of that propeller-driven vehicle relative to the fluid through which it moves; and low advance ratio means low speed of the vehicle. The advance ratio is a means of describing the incoming angle of the fluid relative to the propeller blade. It is analogous to the angle of attack of an airfoil (Ref. 18).

5.7.1 Thrust Coefficient Versus Advance Ratio

Figures 17 shows a plot of thrust coefficient, C_T, as a function of advance ratio, J, for the F31/A31 open rotor model tested at the three simulated flight conditions considered in this work. It is seen that C_T decreases as J is increased. The change in angle of attack and/or presence of pylon seems to have no significant effect on the results.

5.7.2 Input Shaft Power Coefficient Versus Advance Ratio

Figures 18 shows a plot of input shaft power coefficient, C_{sp}, as a function of advance ratio, J, for the F31/A31 model tested at the three simulated flight conditions mentioned before. Just like C_T, C_{sp} also decreases as J is increased. There is little effect on the results with angle of attack change and/or pylon presence.

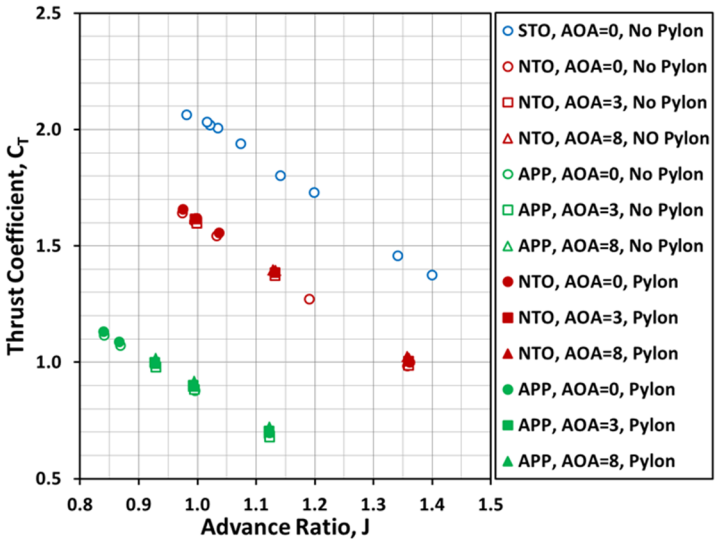

Figure 17.—Plot of C_T versus J for F31/A31 open rotor model.

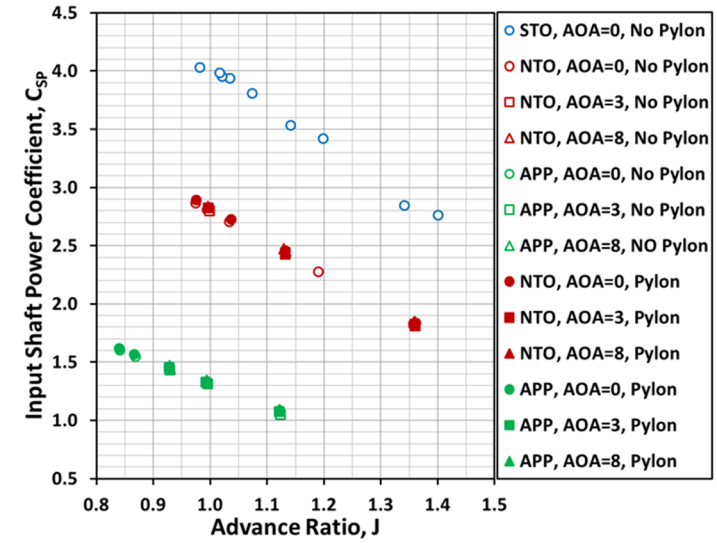

Figure 18.—Plot of C_{sp} versus J for F31/A31 model.

5.7.3 Thrust Coefficient Versus Input Shaft Power Coefficient

Figure 19 shows a plot of C_T versus C_{sp} at the three flight conditions considered for F31/A31 model. As expected, C_T increases with C_{sp}. These results, as noticed, do not fall on a line.

However, by normalizing C_T with J^2, and C_{sp} with J^3, the results can be combined together to get a single curve, as shown in Figure 20, and a correlation between C_T/J^2 and C_{sp}/J^3 can be obtained as:

$$C_T/J^2 = - 0.0460 (C_{sp}/J^3)^2 + 0.6759 (C_{sp}/J^3) + 0.0722 \quad (4)$$

with $R^2 = 0.9993$. This could be a generalized equation for C_T as a function of C_{sp} and J for future open rotor designs similar to F31/A31. The maximum error using this C_T prediction equation is estimated to be less than 2.5 percent.

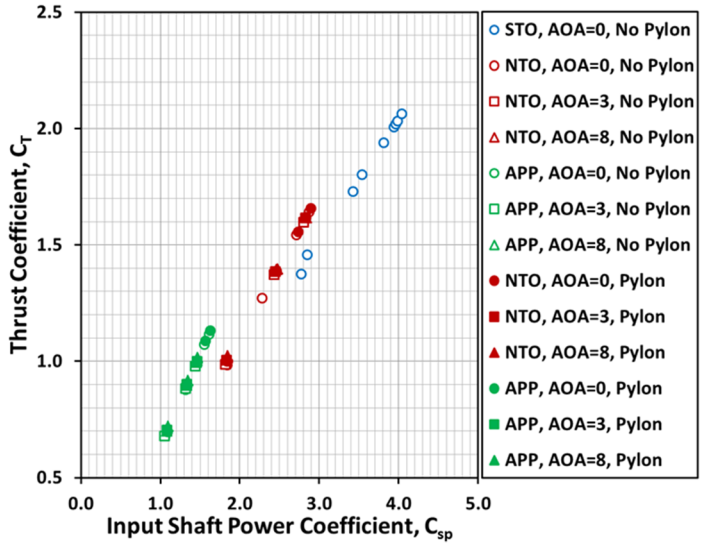

Figure 19.—Plot of C_T versus C_{sp} for F31/A31 model.

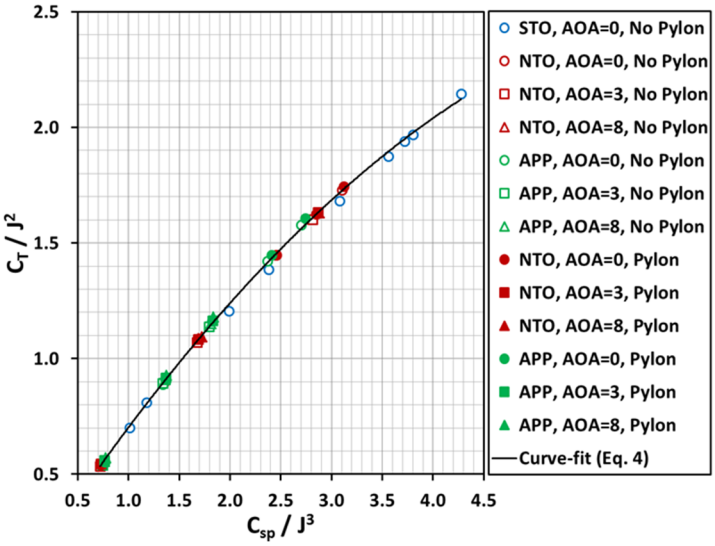

Figure 20.—Plot of C_T/J^2 versus C_{sp}/J^3 for F31/A31 model.

5.7.4 Acoustic Power Coefficient Versus Input Shaft Power Coefficient

A plot of acoustic power coefficient, C_{ac}, versus the input shaft power coefficient, C_{sp}, for the three flight cases of F31/A31 model is shown in Figure 21. Small variations due to the presence of pylon and changes in AOA can be observed in NTO and APP cases. (Recall that the STO case did not have AOA changes or pylon installed.) No reasonable correlation was found for this case.

5.7.5 Propulsion Efficiency Versus Advance Ratio

Figure 22 shows a plot of propulsion efficiency (η_p) as a function of advance ratio, J, for the F31/A31 model tested at all three simulated flight conditions. As noticed, η_p increases as J is increased in each case. Also seen is that, for a given J, η_p decreases as the blade setting angles are increased, i.e., from APP to NTO to STO. Small variations in η_p due to AOA changes and pylon presence can also be observed.

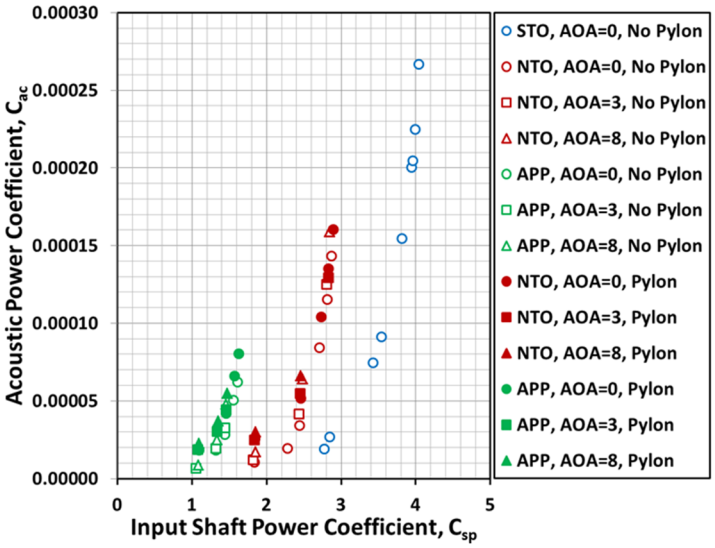

Figure 21.—Plot of C_{ac} versus C_{sp} for F31/A31 model.

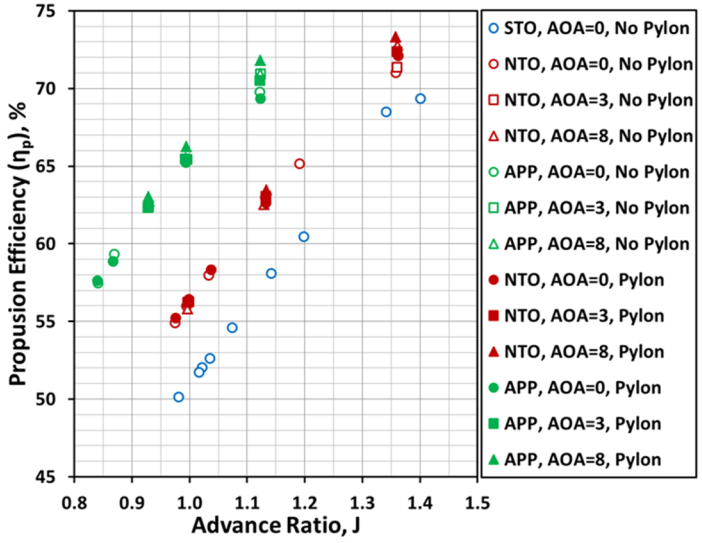

Figure 22.—Plot of η_p versus J for F31/A31 model.

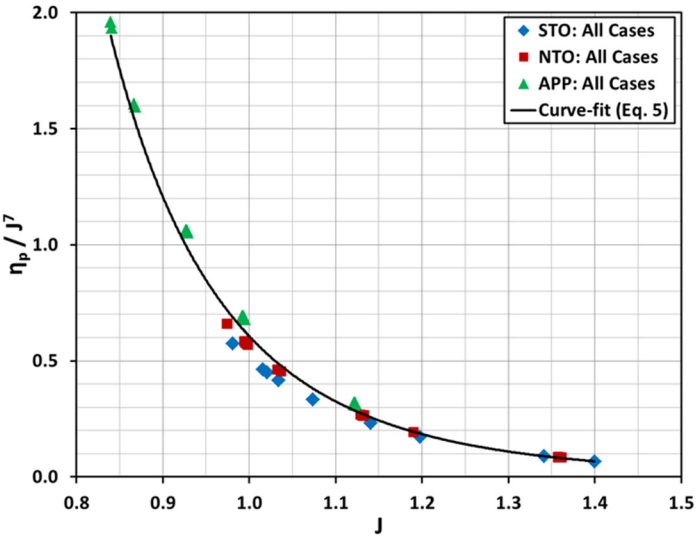

Figure 23.—Plot of η_p/J^7 versus J for F31/A31 model.

The results in Figure 22 can be combined to yield a single curve by plotting η_p/J^7 versus J, as shown in Figure 23. Based on regression analysis, an empirical equation for propulsion efficiency of the F31/A31 model can be obtained as:

$$\eta_p / J^7 = 0.6063\ J^{-6.5363} \text{ or } \eta_p = 0.6063\ J^{0.4637} \tag{5}$$

with $R^2 = 0.9917$. Using this prediction and based on current results, the maximum error in η_p is estimated to be less than 16.5 percent, but it seems rather high.

6.0 Conclusions

Analyses of far-field SPLs, PWLs, and performance characteristics of open rotor model F31/A31 at three simulated flight conditions (STO, NTO, and APP) have been presented in this work. The analyses were performed based on the nonproprietary portion of the test data provided by NASA GRC. Tests cases consisted of variations in rotor speed and angle of attack. An upstream pylon was installed in some cases. All tests were carried out at a freestream Mach number of 0.20 and with both rotors running at the same speed.

A new data analysis technique has been successfully applied to separate the tone and broadband noise components from the measured raw data to understand their level of contribution to total noise. Computed overall, tonal, and broadband SPLs, PWLs, and their variations with rotor speed, angle of attack, thrust, and input shaft power at each simulated flight condition have been presented and discussed. The effect of pylon on the noise levels of the model has been addressed.

The results show that, depending upon rotor design speed and angle of attack, the presence of pylon causes 1 to 5 dB increase in noise level. At any given rotor speed, the STO condition, because of higher thrust involved, shows higher noise level than those at NTO or APP condition. At any given thrust, the APP condition, because of higher speeds involved, shows slightly higher tone noise than those at STO or NTO condition, but, in the case of broadband noise, the opposite happens.

Based on regression analysis, correlations have been developed for relations between thrust and input shaft power, acoustic power and input shaft power, and, propulsion efficiency and advance ratio. The acoustic efficiency of the model is found to be less than 0.007 percent at the three simulated flight conditions.

Finally, it is hoped that the results presented in this work will serve as a good database for comparison and improvement of other open rotor blade designs, as well as for validating open rotor noise prediction codes.

References

1. "Building a Better Plane," NASA News & Features, May 3, 2010, URL: http://www.nasa.gov/topics/aeronautics/features/openrotor_prt.htm [cited 3 May 2010].
2. James, T., "Back to Propellers", Engineering and Technology Magazine, Volume 4, Issue 10, 2 June 2009. URL: http://eandt.theiet.org/magazine/2009/10/back-to-propellers.cfm [cited 2 June 2009].
3. "Fuel prices drive new look at open rotor jet engines," Engineering and Technology Magazine, 27 October 2008. URL: http://eandt.theiet.org/news/2008/oct/open-rotor-test.cfm [cited 27 October 2008].
4. "GE and NASA Partner on Open Rotor Engine Testing," NASA-Ask the Academy, Volume 2, Issue 3, 30 March 2009. URL: http://www.nasa.gov/offices/oce/appel/ask-academy/issues/volume2/AA_2-3_F_ge_rotor.html [cited 30 March 2009].
5. Elliott, D.M., "Initial Investigation of the Acoustics of a Counter Rotating Open Rotor Model with Historical Baseline Blades in a Low Speed Wind Tunnel," *17th AIAA/CEAS Aeroacoustics Conference (32nd AIAA Aeroacoustics Conference)*, Portland, OR, 05 - 08 June 2011.
6. Stephens, D.B., "Data Summary Report for the Open Rotor Propulsion Rig Equipped with F31/A31 Rotor Blades," *NASA/TM—2014-216676*, November 2014.
7. Stephens, D.B., "Nearfield Unsteady Pressure at Cruise Mach Numbers for a Model Scale Counter-Rotation Open Rotor," *18th AIAA/CEAS Aeroacoustics Conference (33rd AIAA Aeroacoustics Conference)*, Colorado Springs, CO, 04-06 June 2012.
8. Woodward, R.P., Hall, D.G., Podboy, G.G., and Jeracki, R.J., "Takeoff/Approach Noise for a Model Counterrotation Propeller with a Forward-Swept Upstream Rotor," AIAA-93-0596, presented at the 31st Aerospace Sciences Meeting & Exhibit, Reno, NV, January 11-14, 1993.
9. Magliozzi, B. and Hanson, D.B. and Amiet, R.K., "Propeller and Propfan Noise," Chapter 1, "Aeroacoustics of Flight Vehicles: Theory and Practice, Volume 1: Noise Sources," NASA-RP 1258, Vol. 1, August 1991.
10. Blandeau, V.P. and Joseph, P.F., "Broadband Noise due to Rotor-Wake/Rotor Interaction in Contra-Rotating Open Rotors," *AIAA Journal*, Vol. 48, No. 11, pp. 2674-2686, November 2010.
11. Parry, A.B., Kingan, M. and Tester, B.J., "Relative Importance of Open Rotor Tone and Broadband Noise Sources," *17th AIAA/CEAS Aeroacoustics Conference (32nd AIAA Aeroacoustics Conference)*, Portland, OR, 05 - 08 June 2011.
12. Sree, D., "A novel signal processing technique for separating tonal and broadband noise components from counter-rotating open-rotor acoustic data," International Journal of Aeroacoustics, Vol. 12, Issue 1/2, June 2013.
13. Sree, D. and Stephens, D.B., "Tone and Broadband Noise Separation from Acoustic Data of a Scale-Model Counter-Rotating Open Rotor," Paper No. AIAA-2014-2744, Proceedings of AIAA Aviation and Aeronautics Forum and Exposition, Atlanta, GA, June 16-20, 2014.
14. Stephens, D.B. and Envia, E. (Acoustics Branch, NASA-GRC, Cleveland, Ohio), Private communications, July 2014.
15. Janardan B.A. and Gliebe P.R., "Acoustic Power Level Comparisons of Model-Scale Counterrotating Unducted Fans," AlAA paper 91-0595, 29th Aerospace Sciences Meeting, Reno, Nevada, January 7-10, 1991.
16. Hanson, D.B., "Sound Power Spectrum and Wave Drag of a Propeller in Flight," AIAA 12th Aeroacoustic Conference, San Antonio, Texas, AIAA 89-1081, April 1989.
17. Huff, D.L., "NASA Glenn's Contributions to Aircraft Engine Noise Research," Journal of Aerospace Engineering, Vol. 26, No. 2, pp. 218-250, April 1, 2013.
18. http://en.wikipedia.org/wiki/Advance ratio.